Journal of Molecular Liquids 361 (2022) 119603

Contents lists available at ScienceDirect

Journal of Molecular Liquids

journal homepage: www.elsevier.com/locate/molliq

Sulfanilic acid-functionalized magnetic GO as a robust adsorbent for the efficient adsorption of methylene blue from aqueous solution

Hassan M.A. Hassan [a], M.R. El-Aassar [a], Mohammed A. El-Hashemy [a], Mohamed A. Betiha [b], Meshal Alzaid [c], Almaha N. Alqhobisi [a], Linah A. Alzarea [a], Ibrahim Hotan Alsohaimi Ph.D. [a,*]

[a] Chemistry Department, College of Science, Jouf University, P.O. Box 2014, Sakaka, Saudi Arabia
[b] Egyptian Petroleum Research Institute, Cairo 11727, Nasr City, Egypt
[c] Physics Department, College of Science, Jouf University, P.O. Box 2014, Sakaka, Saudi Arabia

ARTICLE INFO

Article history:
Received 24 April 2022
Revised 4 June 2022
Accepted 9 June 2022
Available online 13 June 2022

Keywords:
Graphene oxide
Methylene blue
Magnetic nanocomposite
Sulfanilic acid
Adsorption

ABSTRACT

In this work, a superior magnetic graphene oxide (GO) functionalized with sulfanilic acid (Fe_3O_4@GO@SA) was successfully fabricated by an in-situ precipitation approach and amidation reaction as a robust material for methylene blue dye (MB) removal. The obtained material was investigated by different techniques, such as XRD, FTIR, TGA, SEM, zeta potential analysis, and BET analysis. The surface areas of GO, MGO, and the Fe_3O_4@GO@SA nanocomposite were measured to be 3.30, 95.2, and 112 m^2/g, respectively. The particle size of Fe_3O_4@GO@SA was found to be 12.8 nm. The adsorption of MB dye under various adsorption parameters, namely, contact time, temperature, dose, pH, and initial concentration of MB was investigated. The findings revealed that Fe_3O_4@GO@SA possessed good adsorption performance for MB dye under optimal conditions (30.0 mg/dose, 240 min/contact time, pH 8, 298 K/T, and 100 rpm/shaking speed). The adsorption kinetics of Fe_3O_4@GO@SA obeyed pseudo first-order kinetics, and the Langmuir model was the best matched model for MB removal. The highest uptake capacity (q_m) at 298 K was reported to be 317 mg/g. The thermodynamic variables ($\Delta H°$, $\Delta S°$, and $\Delta G°$) suggest that the removal of MB dye using the Fe_3O_4@GO@SA adsorbent is a feasible, exothermic and physical process. Fe_3O_4@GO@SA adsorbs MB molecules via three mechanisms including π-π stacking, columbic attraction, and hydrogen bonding. The Fe_3O_4@GO@SA nanocomposite exhibited good reusability. All the experimental results show that the Fe_3O_4@GO@SA nanocomposite has potential applications in future environmental management.

1. Introduction

Chemically synthesized pigments are complex aromatic materials, and are one of the most dangerous water pollutants to public health and the environment owing to their high toxicological properties [1,2]. Dyes are chemically stable, difficult to decompose, have high toxicity, and are carcinogenic [3,4]. The release of dyes from various industries into the environment without treatment could represent a toxic hazard to human health and the environment. Methylene blue (MB) is a cationic dye, known as basic blue 9, that contains a heterocyclic aromatic chemical compound that turns blue when dissolved in aqueous solutions, and is extensively utilized in a variety of industrial sectors [5]. Excessive exposure to MB causes severe health issues in humans, such as vomiting, skin irritation, raised heart rate, and nausea and it poses toxicity to aquatic organisms [6–8]. Therefore, it is necessary to uptake MB from wastewater prior to being discharged into the environment.

Various physical and chemical methods such as coagulation [9], membrane separation [10], electrochemical oxidation [11], biodegradation [12], photocatalytic degradation [13], chemical oxidation [9], and adsorption [14,15], have been developed. The adsorption method was shown to be a potential approach in the elimination of environmental contaminants due to its simple processing, possibility of using low-cost adsorbents, reusability of the adsorbents, and eco-friendliness [15,16]. Adsorption, among these technologies, remains an excellent approach for removing colors from contaminated water due to its simplicity and inexpensiveness, facile operation, and extensive use.

Recently, the use of graphene oxide (GO) in the removal of pollutants has shown good adsorption properties owing to its large surface area, and superior biocompatibility, and robust chemical, and thermal stability, which makes it highly interesting and favorable for the elimination of contaminants from wastewater [17,18].

* Corresponding author.
E-mail address: ehalshaimi@ju.edu.sa (I.H. Alsohaimi).

https://doi.org/10.1016/j.molliq.2022.119603
0167-7322/

Graphene oxide contains oxygen-rich functional moieties such as carboxyl (–COOH), (C-O-C), (–OH), and (C=O) moieties on its basal planes and at the edges [19]. Modification of GO with different materials such as SiO_2 [20], sand [21], calcium alginate composites [22], CS [23], carboxylated GO [24], and hamnolipids [25], was achieved for the removal of MB from water and showed great efficiency for MB removal. However, these adsorbents face difficulties in separating and recovering the material due to the small particles of GO, which significantly limits their applications in water treatment. Magnetic nanoparticles (Fe_3O_4) have been utilized in various sectors, such as separation of biomolecules, drug delivery, water purification, heterogeneous catalysis, and cancer diagnosis due to their superparamagnetic property which can easily separate analyte molecules from complex systems by using a magnet [26,27]. Therefore, incorporation of Fe_3O_4 nanoparticles onto the GO surface improves the separation of the material by an external magnetic field [28,29]. Introducing or modifying functional moieties on the surface of magnetic GO improves the removal capacity toward pollutants. Tran et al., synthesized a Fe_3O_4@CS@G hybrid by a facile precipitation method and utilized it for the uptake of MB from an aqueous medium. They found that the uptake capacity of FCG toward MB dye was 181 mg/g [30].

Sulfanilic acid or 4-amino-1-naphthalenesulfonic [$H_2NC_{10}H_6SO_3H$] is an amino acid aniline derivative. Sulfanilic acid (SA) is widely used as a small molecular catalyst in the asymmetric synthesis of organic compounds [31]. SA contains amino (–NH_2) and sulfonyl (-SO_3H) groups which can form stable chelates with pollutants [32]. Therefore, sulfanilic acid-functionalized magnetic graphene oxide may enhance the adsorption capacity of the Fe_3O_4@GO@SA hybrid toward MB dye. In the previous literature, the modification of magnetic graphene oxide with sulfanilic acid has not been conducted for the removal of MB from an aqueous solution.

In this study, a unique magnetic nanocomposite (Fe_3O_4@GO@SA) was fruitfully fabricated by the following process: GO was first fabricated by a modified Hummers' approach and Offeman approach, and then Fe_3O_4 graphene oxide (Fe_3O_4@GO) was synthesized through-loading magnetic nanoparticles on the GO surfaces by a chemical in situ coprecipitation method. After that, the carboxylic groups of Fe_3O_4@GO were reacted with the amino group of sulfanilic acid (SA) to produce a new magnetic nanocomposite (Fe_3O_4@GO@SA). The Fe_3O_4@GO@SA nanocomposite was investigated by various techniques, such as XRD, FTIR, SEM, TGA, and zeta potential analysis. The optimization of all parameters, such as the dose of adsorbent, initial concentration of MB, adsorption time, pH, and temperature were investigated. Different kinetic models and adsorption isotherms were also investigated. The recycling of the Fe_3O_4@GO@SA adsorbent was successfully achieved.

2. Experimental

2.1. Materials

All of the materials were of analytical quality and were utilized without additional treatment. HNO_3 (70%), HCl (36.5–38.0%), and NH_4OH (25%) were purchased from BDH Chemicals Ltd. (Poole, England). Sulfanilic acid (SA, ≥ 99.0%), $SOCl_2$, (≥99.0%), $FeCl_2{\cdot}4H_2O$ (≥99.0%), $FeCl_3{\cdot}6H_2O$ (≥99.0%), and methylene blue (MB) were provided by Sigma Aldrich.

2.2. Fabrication of Fe_3O_4@GO@SA

2.2.1. Fabrication of Fe_3O_4@GO

Graphene oxide (GO) was synthesized by a modified Hummers' approach and Offeman approach [33]. The resulting powder cake was rinsed with hot water many times and then separated and dried at 25 °C for 12 hrs. Chemical in situ precipitation methods were used to deposit magnetite nanoparticles on the graphene oxide surfaces. First, 5.42 g of $FeCl_3{\cdot}6H_2O$ and 1.99 g of $FeCl_2{\cdot}4H_2O$ at a molar ratio of 2:1 was dissolved in a 0.100 M HCl solution under N_2 gas. After stirring for approximately 30 min, 1.20 g of GO was added to a mixture of ferric and ferrous salts and stirred at 75 °C for 30 min. Then, ~40.0 mL of NH_4OH solution was introduced dropwise into the mixture solution under mechanical stirring and N_2 gas (to prevent oxidation of Fe_3O_4) until the pH reached ~ 10. After that, the obtained Fe_3O_4@GO was isolated by a magnet, rinsed, and vacuum dried for 24 h at 60 °C (Scheme 1).

2.2.2. Synthesis of Fe_3O_4@GO@SA

Fe_3O_4@GO@SA was prepared via the amidation reaction of Fe_3O_4@GO with sulfanilic acid using $SOCl_2$. In a typical procedure, a mixture of Fe_3O_4@GO (2.00 g) and a slight excess of thionyl chloride (3.00 mL) was heated under stirring at 70 °C for 4 h. After cooling, the resulting dark greenish product was filtered and dried. A total of 1.00 g of acid chloride in magnetic graphene oxide was dispersed in 20.0 mL of DMF. The blend was refluxed for 4 h at 80 °C. After the reaction was completed, the blend was cooled and then isolated by a magnet, rinsed with deionized water many times, and then vacuum dried for 24 h at 60 °C (Scheme 1).

2.2.3. Adsorption assessment

Batch-method adsorption studies were performed using the Fe_3O_4@GO@SA nanocomposites as adsorbents to eliminate MB dye from aqueous solutions. To determine the optimum adsorption conditions, experiments were carried out using different pH values (2–8), contact times (1–1440 min), initial concentrations of MB (33.5–300 mg/L), adsorbent mass (10.0–50.0 mg), and temperatures (25.0–45.0 °C). The batch experiments were performed using a 100 mL Erlenmeyer flask with the addition of 30 mg of Fe_3O_4@GO@SA and 50 mL of MB solution with an initial concentration of 33.5 mg/L. Then, the desired pH was adjusted with HCl (0.1 M) or NaOH (0.100 M). After that, the solutions were agitated at 100 rpm for a desired time, and then separated by the aid of a magnet. The remaining MB concentrations were determined utilizing a UV/Vis spectrophotometer at 665 nm. The percentage of adsorption (R_e %) and the adsorption amount (q_e, mg g^{-1}) were assessed by Eqs. (1) and (2), respectively:

$$R_e\,(\%) = \frac{C_o - C_e}{C_o} \times 100 \quad (1)$$

$$q_e = \frac{(C_o - C_e)V}{m} \quad (2)$$

where C_o (mg/L) and C_e (mg/L) are the initial and equilibrium concentrations of MB in the solution, respectively; m is the Fe_3O_4@GO@SA mass; and V (L) is the MB volume solution.

The reusability of the Fe_3O_4@GO@SA nanocomposite for MB dye adsorption was investigated. After the adsorption experiments, the MB-loaded Fe_3O_4@GO@SA nanocomposites were magnetically separated and the MB concentration in the supernatant was determined. The MB-loaded Fe_3O_4@GO@SA adsorbent was then treated with 50 mL of NaOH (0.01 M), HCl (0.01 M), and HNO_3 (0.01 M) and then shaken separately for 240 min. After that, the adsorbent was collected by a magnet. This run was repeated four times. The percentage of MB desorption was determined using Eq. (3).

$$\%\,\text{desorption} = \frac{C_m}{C_e} \times 100 \quad (3)$$

where C_m and C_e are the desorbed MB concentration and the initially adsorbed MB concentration, respectively (Fig. 1).

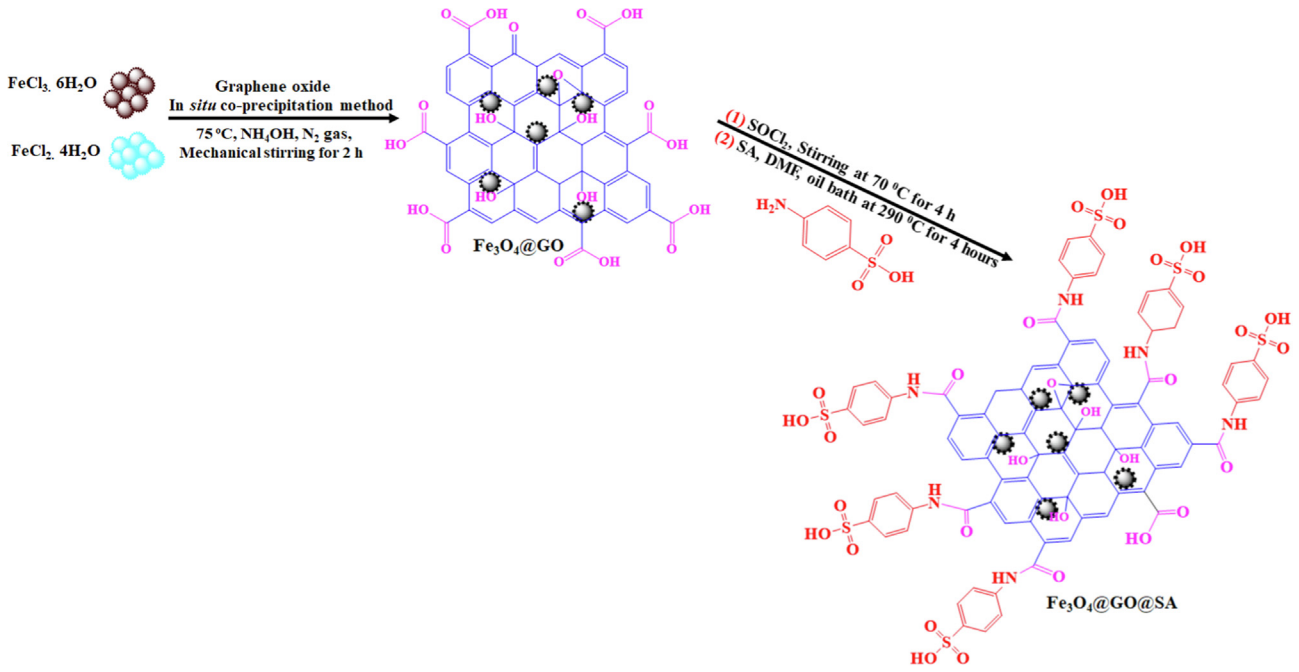

Scheme 1. Schematic representation of the preparation processes of Fe_3O_4@GO@SA nanocomposite.

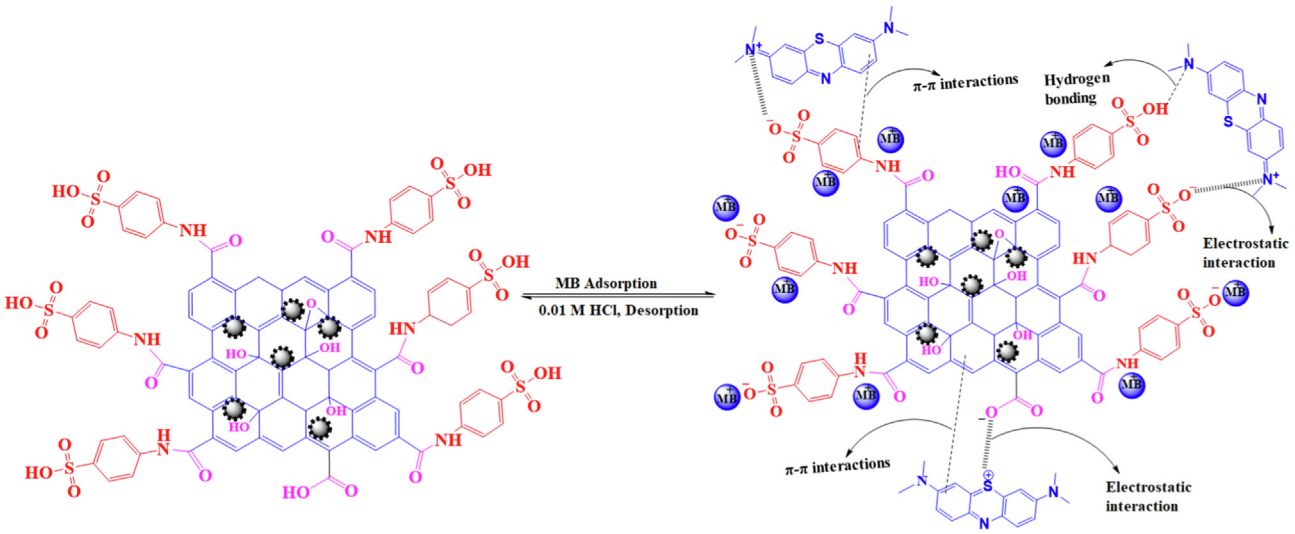

Fig. 1. Mechanism adsorption of MB using of Fe_3O_4@GO@SA adsorbent.

3. Results and discussion

3.1. Characterization

The X-ray diffraction patterns of GO, Fe_3O_4@GO, and Fe_3O_4@GO@SA were obtained on a Maxima = X diffractometer (D/Max2500VB2+/Pc, Shimadzu Company, Japan) with an X-ray wavelength Cu detector. The morphology of GO, Fe_3O_4@GO, and Fe_3O_4@GO@SA was characterized by a scanning electron microscope (Quattro S, Thermo Scientific). FTIR spectra of GO, Fe_3O_4@GO, and Fe_3O_4@GO@SA were obtained with a Shimadzu IR Tracer-100. The zeta potential of Fe_3O_4@GO@SA was obtained by a Zetasizer Nano ZS instrument (Malvern, UK). TGA analyses of GO, Fe_3O_4@GO, and Fe_3O_4@GO@SA were performed using a TGA-51 Shimadzu TGA analyser.

To explore the surface characteristics of GO, Fe_3O_4@GO, and Fe_3O_4@GO@SA, FTIR analysis was carried out, as shown in Fig. 2**a**. For GO, several characteristic bands were observed; for example the bands at 3444, 1719, 1622, 1370, 1240 cm^{-1}, and 1160–1027 cm^{-1} were ascribed to the stretching mode of hydroxyl (O–H), C=O group in carbonyl moieties and COOH, C=C, O–H deformation mode, and stretching of C–O-C, respectively [34,35]. An additional peak at 555 cm^{-1} was assigned to the stretching mode of the Fe-O bond, which confirms the formation of magnetic graphene oxide (MGO) [36]. The broad band in the region of 3150–3354 cm^{-1} in the Fe_3O_4@GO@SA spectrum is related to the overlap of NH/OH moieties, [37]. The peaks at 3059 and 2865 cm^{-1}correspond to the aromatic C-H symmetric and antisymmetric vibrations, respectively. The peak at 1650 cm^{-1} is assigned to amide 1 (NHCO) [37]. The peak at 1573 cm^{-1} is due to secondary amide 2

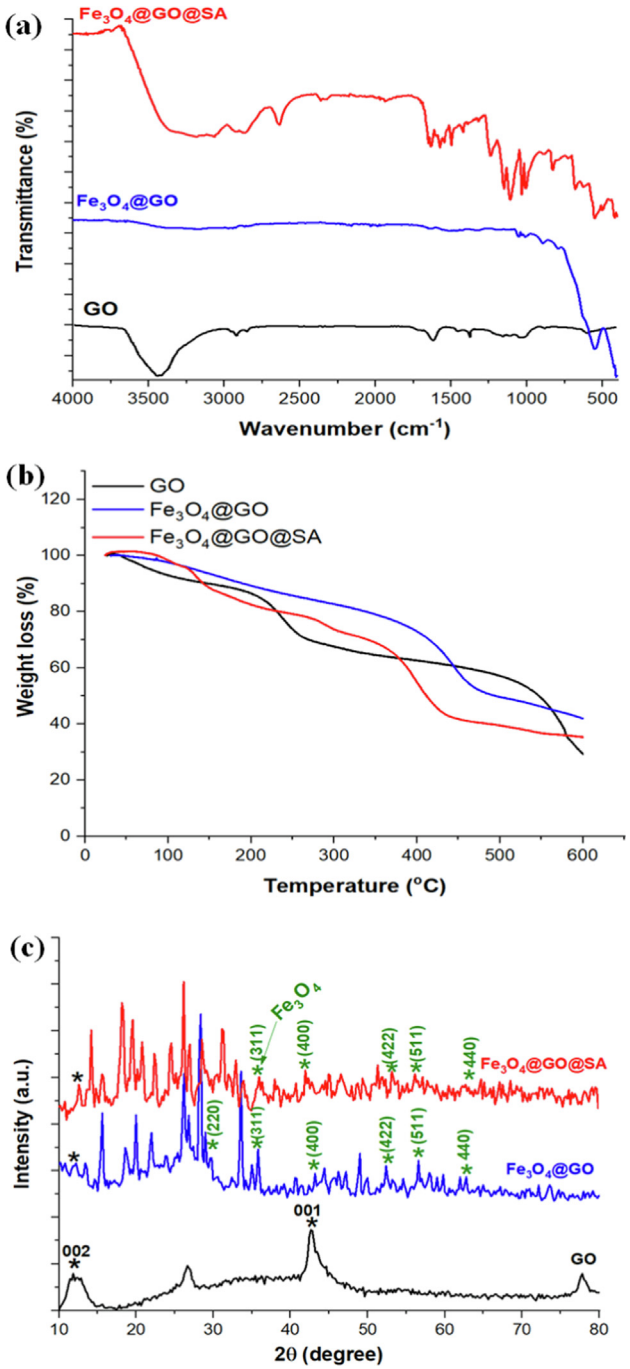

Fig. 2. FTIR spectra (a), TGA analysis (b), and XRD pattern of GO, Fe_3O_4@GO, and Fe_3O_4@GO@SA.

(N–H bending), indicating the formation of an amide bond between the COOH moiety of the Fe_3O_4@GO surface and the NH_2 group of the SA surface. The peaks in the range of 1008–1034 cm^{-1} and at 1419 and 1150 cm^{-1} are due to symmetric stretching of the S-O bond and stretching of the SO_3 group in the SA [38,39] which confirms the successful formation of Fe_3O_4@GO@SA. The peak at 559 cm^{-1} was ascribed to the unique band of the Fe-O stretching mode, indicating the development of magnetic nanoparticles [40,41]. The peaks at 1495, 1388 cm^{-1}, 1240, and 677 cm^{-1} were ascribed to ring stretching (C=C), ν(C-N), ν (C-O), and special stretching of C–S, respectively [39,42]. In conclusion, the FTIR results successfully confirmed the formation of Fe_3O_4@GO@SA.

The thermal stabilities of GO, Fe_3O_4@GO, and Fe_3O_4@GO@SA were determined via TGA as presented in Fig. 2**b**. The TGA curves of GO, Fe_3O_4@GO, and Fe_3O_4@GO@SA showed that losses of ~ 70.0%, ~56.0%, and ~ 61.0%, respectively, in three steps. In the first step, weight losses of ~ 10.0%, ~7.00%, and ~ 10.0% were found in the temperature range of 30–150 °C for GO, Fe_3O_4@GO, and Fe_3O_4@GO@SA, respectively, which are related to the moisture content [43]. The second and third steps were from 150 to 250 °C and from 250 to 580 °C, respectively, where ~ 20.0% and 40.0% weight losses occurred due to the degradation of the labile oxygen functional moieties of GO [44]. For Fe_3O_4@GO, the weight losses of 10.0% and 36% from 150 to 300 °C and from 300 to 550 °C can be ascribed to the decomposition of oxygen-containing functional moieties such as COOH and C=O moieties, respectively [44]. Approximately ~ 22.0 % and ~ 30.0 % weight losses were observed in the temperature ranges of 150 to 300 °C and 300 to 550 °C for Fe_3O_4@GO@SA, respectively, owing to the degradation of the functional groups of organic molecules (SA and GO). Compared with the weight loss of GO at 500 °C, the weight loss of Fe_3O_4@GO@SA is much higher, indicating the successful formation of Fe_3O_4@GO@SA.

Fig. 2**c** illustrates the XRD patterns of GO, Fe_3O_4@GO, and Fe_3O_4@GO@SA. For GO, the characteristic peaks observed at 2θ = 11.9° and 43.4° were attributed to the (002) and (100) planes, respectively. These peaks were reduced in Fe_3O_4@GO, and Fe_3O_4@GO@SA [40,43]. The diffraction peaks at 2 θ = 35.9° (311), 43.1° (400), 53.4° (422), 56.8° (511), and 63.1° (440) in Fe_3O_4@GO and Fe_3O_4@GO@SA were assigned to the refection planes of the cubic spinel crystal structure of magnetite, indicating the existence of Fe_3O_4 nanoparticles in the as-prepared adsorbent [41,45]. The other peaks in Fe_3O_4@GO@SA are due to the crystallinity of SA [46]. The particle size of Fe_3O_4@GO@SA was calculated by the Scherer equation [47] at 2θ = 35.9° and the result revealed that the particles were 12.8 nm in size. This value is greater than those of pure Fe_3O_4 reported the literature [40].

The morphological features of GO, Fe_3O_4@GO, and the Fe_3O_4@GO@SA nanocomposite were examined by FESEM, and the findings are illustrated in Fig. 3. It was noted that the SEM image of graphene oxide shows layers with wrinkled edges and smooth surfaces (Fig. 3**a**). For Fe_3O_4@GO, the magnetic nanoparticles are spherical, aggregated, and of high density on the GO surface (Fig. 3**b**). The adsorbent surface becomes smooth with cracks and irregular pores as indicated in Fig. 3**c**. The BET surface areas surface area of GO, MGO, and the Fe_3O_4@GO@SA nanocomposite were found to be 3.30, 95.2, and 112 $m^2 \cdot g^{-1}$, respectively.

3.2. Adsorption performance of Fe_3O_4@GO@SA

3.2.1. Influence of solution pH

The capabilities of Fe_3O_4@GO@SA for MB adsorption were achieved at various pH values (2–8) while keeping all other parameters constant (0.0300 g, 33.5 mg/L, 25 °C, 24 h, and 100 rpm) (Fig. 4**a**). It is worth noting that the capacity of Fe_3O_4@GO@SA for MB removal was boosted from 2.53 to 50.5 mg/g when the pH increased from 2 to 8. This behavior can be clarified based on the protonation and deprotonation of different surface functional groups of the MB molecule and the Fe_3O_4@GO@SA adsorbent. In an acidic medium, the number of hydronium ions (H_3O^+) in the solution increases, and the functional groups (SO_3H, COOH, and OH) on the Fe_3O_4@GO@SA surface become positive, which would electrostatically repel positively charged cationic MB, resulting in a reduction in the adsorption capacity of Fe_3O_4@GO@SA toward MB. However, at a higher pH range, the adsorption capacities were enhanced owing to the deprotonation of SO_3H, COOH, and OH groups, which enhanced the charge density and thus strengthened

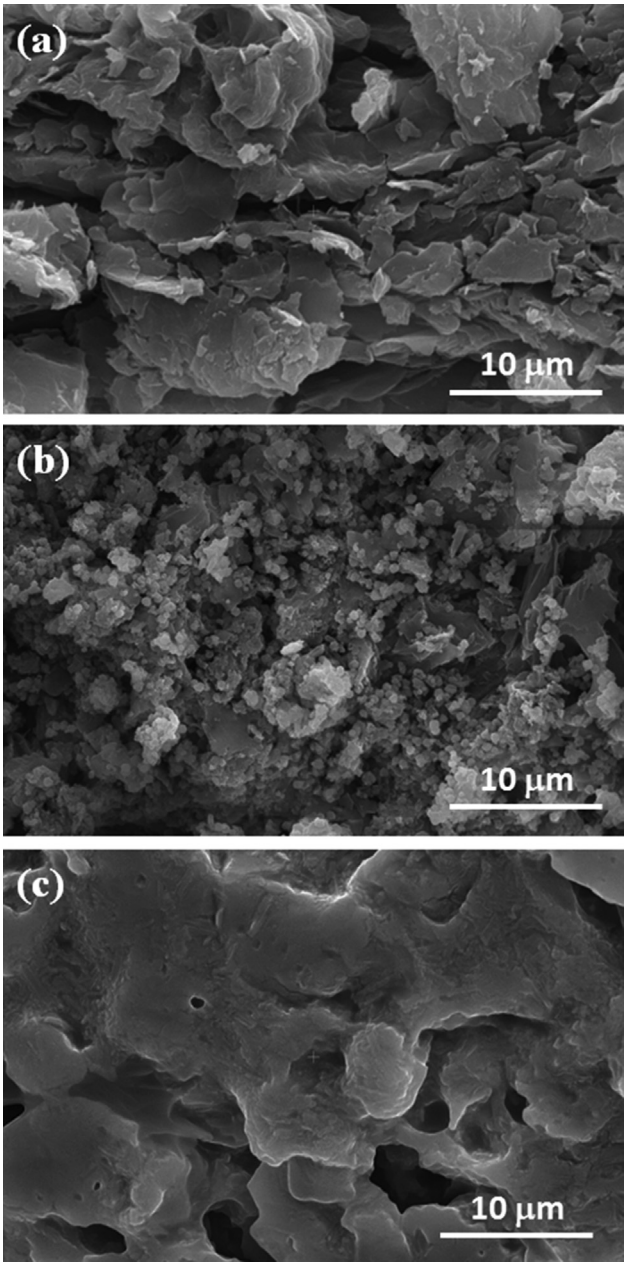

Fig. 3. SEM images of GO (a), Fe_3O_4@GO (b), and Fe_3O_4@GO@SA.

the columbic interaction between Fe_3O_4@GO@SA and the cationic MB molecule dye, resulting in the improved adsorption performance of Fe_3O_4@GO@SA toward MB. In addition, when the pH > 8, the adsorption capacity of Fe_3O_4@GO@SA exhibited a reduction owing to the decomposition of MB dye as reported in the literature [48].

Evaluation of the surface charge of Fe_3O_4@GO@SA through zeta potential measurement at different pH values indicates that the zero-point charge (pH_{pzc}) of the Fe_3O_4@GO@SA nanocomposite is ~ 4.60 (Fig. 4**b**). This means that at pH < pH_{pzc} (pH_{pzc} = 4.60) the Fe_3O_4@GO@SA surfaces are positively charged owing to the protonation of functional moieties on the Fe_3O_4@GO@SA surface ($-SO_3H_2^+$, $-COOH_2^+$, and $-OH_2^+$), which reduces the cationic MB adsorption on the Fe_3O_4@GO@SA surface. When the pH exceeds pH_{pzc}, the surface gains a negative charge due to the deprotonation of functional groups on the Fe_3O_4@GO@SA surface ($-SO_3^-$, and $-COO^-$), which enhances the cationic MB adsorption on the Fe_3O_4@GO@SA surface by the electrostatic attraction force [49]. Hence, in the subsequent investigations, all adsorption experiments were performed at pH = 8.

3.2.2. Impact of adsorbent dose

The impact of adsorbent dosage on MB uptake onto the Fe_3O_4@GO@SA nanocomposite was examined by altering the adsorbent dosage from 10 mg to 50 mg while keeping all other parameters constant (33.5 mg/L, 24 h, 25 °C, pH 8, and 100 rpm), as displayed in Fig. 5**a.** With the increase in the amount of Fe_3O_4@GO@SA nanocomposite from 10 to 30 mg, the removal efficiency increased from 75.5% to 9.20%. With the further increase of Fe_3O_4@GO@SA loading to 50.0 mg, the removal efficiency became nearly constant mainly due to the active sites being enhanced with the increased amount of the Fe_3O_4@GO@SA nanocomposite. On the other hand, the adsorption capacity of Fe_3O_4@GO@SA nanocomposite toward MB dye was reduced to 30.9 mg/g with an increase in the dose to 50.0 mg. This is because the adsorbent mass is inversely proportional to the unit adsorption capability in the adsorption capacity equation. In addition, aggregation of the Fe_3O_4@GO@SA adsorbent at a high dosage decreases the adsorbent's surface area and reduces its adsorption capability [15]. Hence, in the subsequent investigations, all adsorption experiments were performed using 30.0 mg of Fe_3O_4@GO@SA.

3.2.3. Influence of contact time

The impact of adsorption time on the adsorption capacity of Fe_3O_4@GO@SA adsorbent toward MB dye was carried out in the time range of 1–1440 min while keeping all other factors constant (33.5 mg/L, 30.0 mg, pH 8, 25 °C, and 100 rpm) (Fig. 5**b**). The

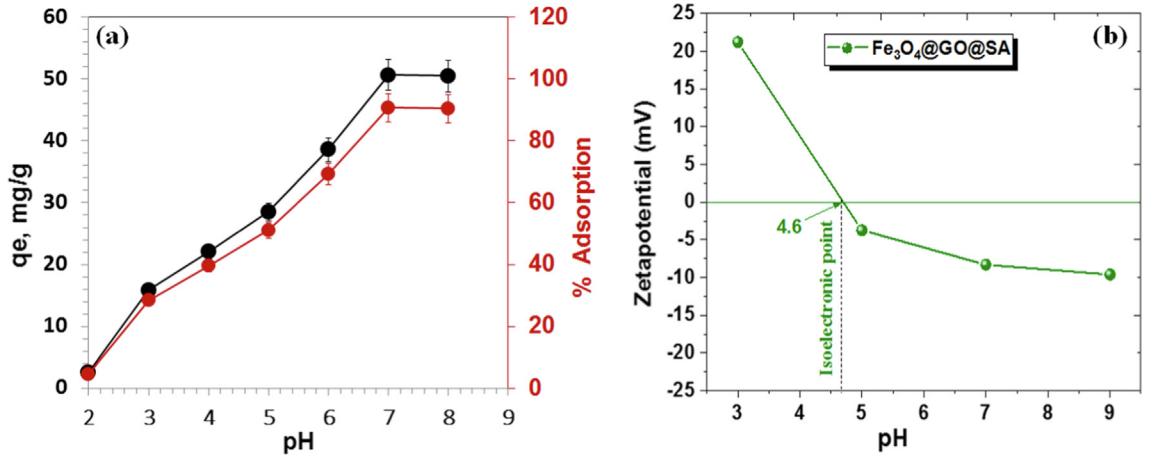

Fig. 4. Effect of solution pH on adsorption of MB dye onto Fe_3O_4@GO@SA (a) Zeta potential measurements of Fe_3O_4@GO@SA at different pH values (b).

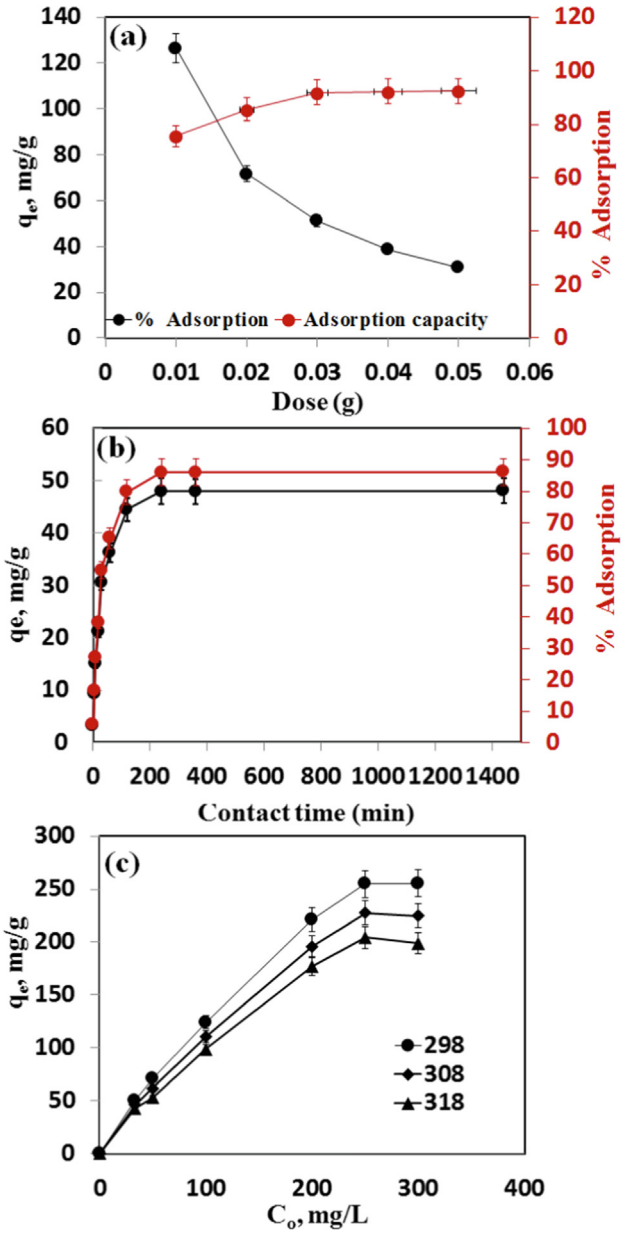

Fig. 5. Effect of adsorbent mass (a), contact time (b), and initial MB concentration on adsorption of MB dye onto Fe_3O_4@GO@SA (c).

removal capability of Fe_3O_4@GO@SA toward methylene blue rises rapidly at the early contact time and the adsorption tends to balance gradually in the later stage. The removal capacity reached equilibrium up to 48.9 mg at 240 min. The increase in the removal capacity of Fe_3O_4@GO@SA toward MB during the initial period of contact time is due to a great number of active adsorption centers on the Fe_3O_4@GO@SA hybrid [50]. Therefore, 240 min was selected as the suitable adsorption time for MB molecules.

3.2.4. Influence of the initial concentration of MB

The impact of the initial MB concentration on MB removal by the Fe_3O_4@GO@SA hybrid was investigated in the range of 33.5–300 mg/L at various temperatures 25–45 °C under the parameter conditions of 30.0 mg, 240 min, pH 8, 25 °C, and 100 rpm (Fig. 5**c**). The removal capability of Fe_3O_4@GO@SA toward methylene blue at 25 °C steadily increased from 50.1 to 256 mg/g with increasing the MB dye concentration from 33.5 to 250 mg/L and then reached adsorption saturation at 300 mg/L. This result reveals that the active adsorption sites (SO_3^-, and COO^-) on Fe_3O_4@GO@SA have strong electrostatic interactions with the cationic MB dye [51]. Regarding the effect of temperature on MB adoption, the findings reveal that the removal capacity of Fe_3O_4@GO@SA was decreased from 50.1 to 43.0 mg/g and 256 to 199 mg/g with increasing temperature from 25 to 45 °C at 33.5 and 300 mg/L, respectively, which confirmed that the removal process is exothermic [52]. Therefore, T = 25 °C was selected as the suitable temperature for MB adsorption onto the Fe_3O_4@GO@SA adsorbent. A similar impact of temperature on the uptake of MB was reported in other studies [53,54].

3.3. Adsorption isotherm

To explore the correlation between MB dye adsorption on the Fe_3O_4@GO@SA adsorbent and its residual concentration in solution, two isotherm models, the Freundlich model in Eq. (4) [55] and the Langmuir model in Eq. (5) [56], were applied:

$$q_e = K_F C_e^{1/n} \tag{4}$$

$$q_e = \frac{q_m K_L C_e}{1 + K_L C_e} \tag{5}$$

where Ce, q_e, and q_m are the equilibrium MB concentration (mg/L), and, equilibrium, and maximum adsorption capacities (mg/g), respectively; K_L is the Langmuir constant (L mg^{-1}) related to the adsorption energy; K_F is the Freundlich constant ((mg g^{-1}) (L $mg^{-1})^{1/n}$) attributed to the adsorption capacity; and n is the heterogeneity factor reflecting the adsorption intensity in which $0 < n < 10$ indicates favorable adsorption. The fitting results and parameters obtained from the isotherms are presented in Fig. 6 and Table 1. The R^2 coefficient of the Langmuir model (R^2 = 0.980) was higher than that of the Freundlich model (R^2 = 0.971); therefore, the Langmuir model was suitable for describing MB adsorption on Fe_3O_4@GO@SA, indicating that the adsorption of MB onto the Fe_3O_4@GO@SA nanocomposite is monolayer coverage. The maximum monolayer capacity of the Fe_3O_4@GO@SA nanocomposite toward MB dye was found to be 317 mg/g, which was higher than those of other adsorbents, such as magnetic chitosan composite (33.2 mg/g) [57], magnetic iron oxide (25.5 mg/g) [58], magnetic humic acid/graphene oxide composite (59.0 mg/g) [48], PANI/RGO(19.2 mg/g) [59], magnetic graphene oxide modified zeolite (97.3 mg/g) [60], magnetite/rGO (145 mg/g)[61], β-cyclodextrin modified magnetic graphene oxide (94.0 mg/g) [43], tannic acid@Fe_3O_4(91.0 mg/g) [62], manganese ferrite/graphene oxide (89.3 mg/g) [63], and Fe_3O_4/chitosan/-graphene nanocomposite (47.4 mg/g) [64] (Table 2). It can be observed that Fe_3O_4@GO@SA displays a robust MB removal performance. In addition, the values of the dimensionless separation factor (R_L) were found to be in the range of 0.500–0.700, which suggested that MB adsorption using the Fe_3O_4@GO@SA nanocomposite is favorable.

3.4. Adsorption kinetics

The experimentally collected kinetic adsorption data were fitted into two nonlinear kinetic models; the pseudo first-order (PFO) model in Eq. (6) [65] and the pseudo second-order (PSO) model in Eq. (7).

$$q_t = q_e(1 - e^{-k_1 t}) \tag{6}$$

$$q_t = \frac{q_e^2 k_2 t}{1 + q_e k_2 t} \tag{7}$$

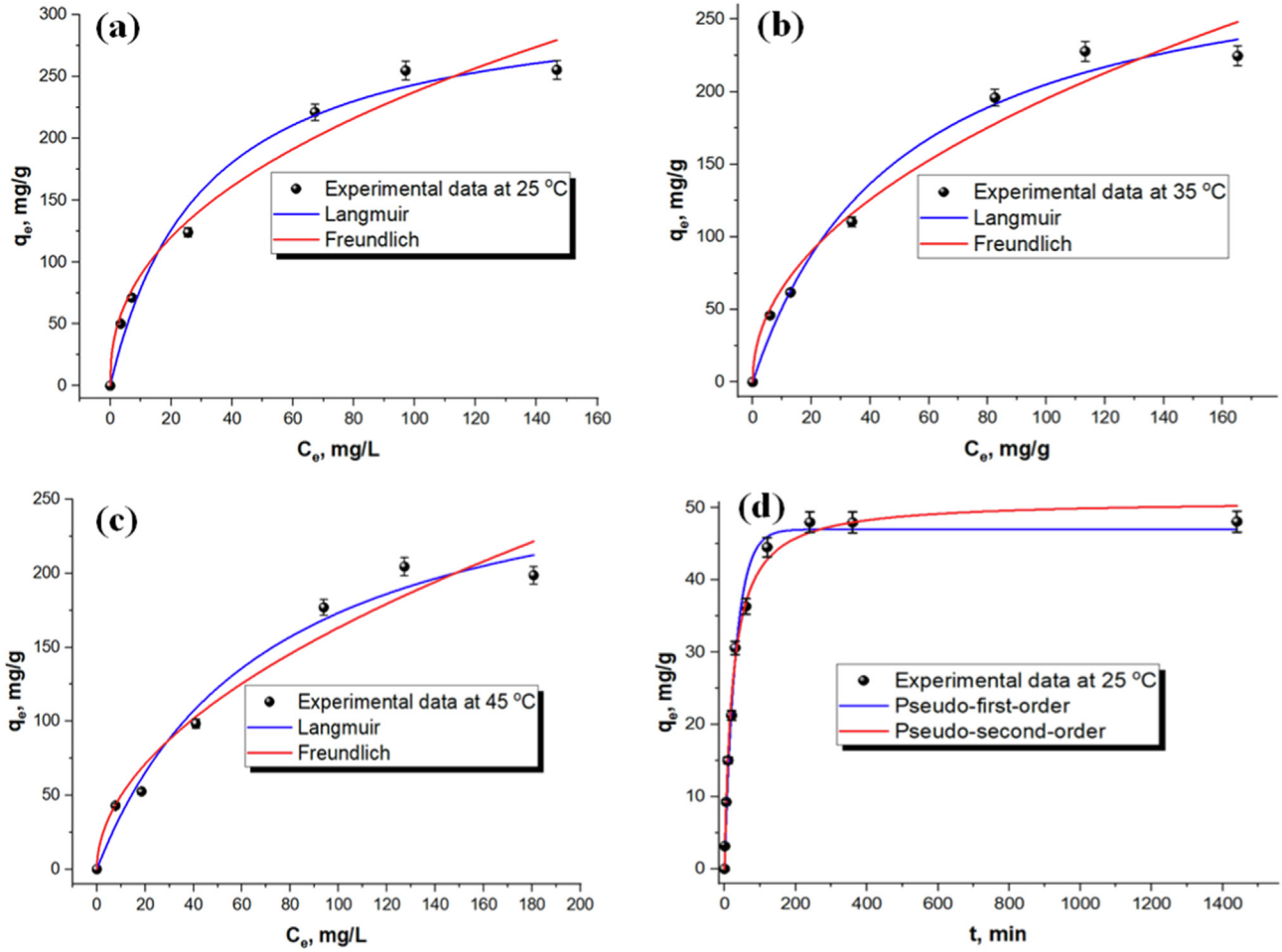

Fig. 6. Non-linear fitted isotherm models for the MB adsorption onto Fe_3O_4@GO@SA at different temperature 25 °C (a), 35 °C (b), 45 °C (c), and Non-linear fitted kinetic models for the MB adsorption onto Fe_3O_4@GO@SA at 25 °C (d).

Table 1
Langmuir and Freundlich isotherms models for MB adsorption on Fe_3O_4@GO@SA nanocomposite.

Model	MB		
	298 K	**308 K**	**318 K**
Langmuir			
q_m, mg/g	317	308	295
K_L (L/mg)	0.0330	0.0201	0.0140
R_L	0.500	0.600	0.700
R^2	0.980	0.983	0.976
Freundlich			
K_f, (mg/g) $(L/mg)^{1/n}$	33.8	21.5	15.2
n	2.40	2.10	1.94
R^2	0.971	0.970	0.960

Table 2
Maximum adsorption capacity (q_m) of various magnetic nanocomposite absorbents of MB.

Adsorbent	**q_m (mg/g)**	**Kinetic models**	**Isotherm models**	**Reference**
Magnetic chitosan composite	33.2	Pseudo-second-order	Langmuir	[55]
Magnetic iron oxide	25.5	Pseudo-second-order	Langmuir	[56]
Magnetic humic acid/graphene oxide composite	59.0	Elovich	Langmuir	[46]
PANI/RGO	19.2	Pseudo-first-order	Langmuir	[57]
Magnetic graphene oxide modified zeolite	97.3	Pseudo-second-order	Freundlich	[58]
Magnetite/rGO	144	Pseudo-first-order	Langmuir	[59]
β-cyclodextrin modified magnetic graphene oxide	94.0	Pseudo-first-order	Langmuir	[41]
Tannic acid@Fe_3O_4	91.0	Pseudo-second-order	Langmuir	[60]
Manganese ferrite/graphene oxide	89.2	Pseudo-second-order	Langmuir	[61]
Fe_3O_4/chitosan/graphene nanocomposite	47.3	Pseudo-first-order	–	[62]
Fe_3O_4@GO@SA	317	Pseudo-first-order	Langmuir	This study

Table 3
Pseudo-first-order and Pseudo-second-order kinetics models for MB adsorption on Fe_3O_4@GO@SA nanocomposite.

C_o (mg/L)	$q_{e,exp.}$ (mg/g)	***Pseudo-first-order***			***Pseudo-second-order***		
		$q_{e1,\ cal.}$ (mg/g)	K_1 (1/min)	R^2	$q_{e2,\ cal.}$ (mg/g)	K_2 (g/mg-min)	R^2
33.5	48.0	47.0	0.0321	0.994	51.1	8.51E-4	0.990

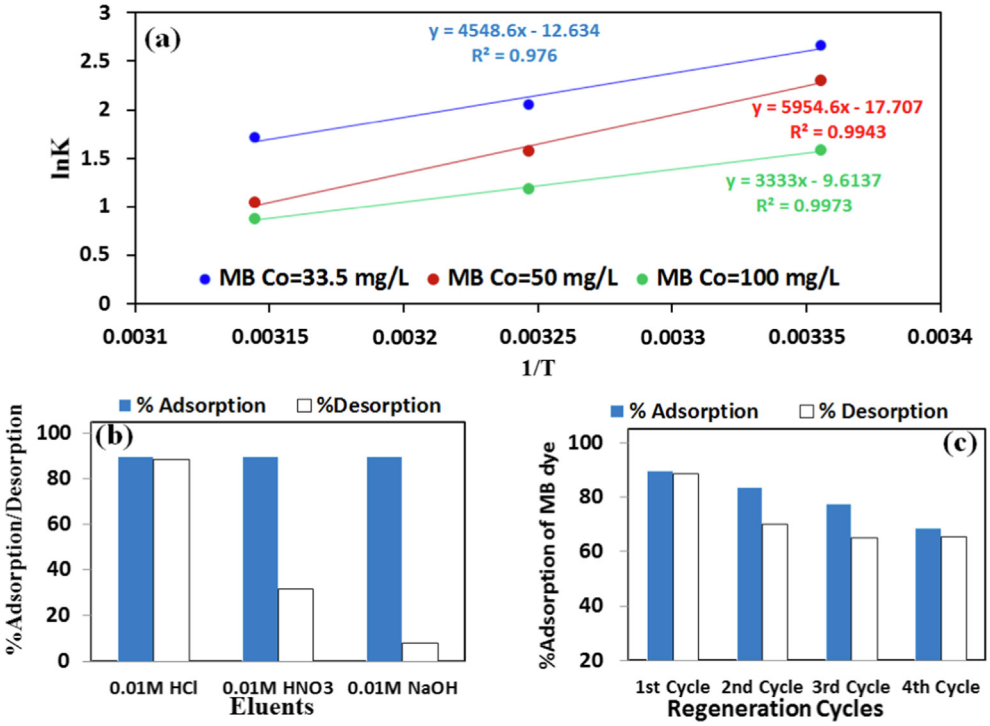

Fig. 7. Plot of ln K vs. 1/T for thermodynamic parameters calculation(a), Desorption study (b), and reusability of Fe_3O_4@GO@SA (c).

where qt (mg/g) is the equilibrium adsorption capacity at time t and k1 (min^{-1}) and k2 are the PFO and PSO(g/mg*min) constants, respectively. Fig. 6**d** and Table 3 show the fitting findings and variables obtained from the kinetics models. Compared with the PSO model (R^2 = 0.990), the PFO model possesses a better regression coefficient (R^2 = 0.994), indicating that the adsorption of MB onto Fe_3O_4@GO@SA is physical adsorption through electrostatic attractions between the negative charges of -SO_3H, COOH, and OH on the adsorbent surface and $^+N(CH_3)_2$ in the MB molecule. In addition, π-π connections between the adsorbent benzene ring and MB molecules are illustrated in Fig. 1. The assessed q_e value ($qe,_{cal}$ = 38.3 mg/g) from the pseudo second-order model does not match the experimental results ($qe,_{exp}$ = 48.0 mg/g). This result indicated that the adsorption process followed the PFO kinetic model.

3.5. Thermodynamic variables

To explore the feasibility of MB uptake by the Fe_3O_4@GO@SA nanocomposite, the thermodynamic variables ΔG° (Eq. (8)), ΔH° (Eq. (9)), and ΔS° (Eq. (9)) were determined.

$$\Delta G^{\circ} = -RTlnKc \tag{8}$$

$$lnKc = \tag{9}$$

where R is the universal gas constant (8.314 J/(mol·K)); T is the temperature in Kelvin; and Kc is the thermodynamic constant, which is equal to q_e/C_e. The ΔH° and ΔS° of the removal process were estimated from the intercept and slope of the plot of ln Kc against 1/T (Fig. 7**a**). Table 4 depicts the thermodynamic variables for MB uptake on the Fe_3O_4@GO@SA hybrid. The negative values of

Table 4
Thermodynamics parameters for the adsorption of MB on Fe_3O_4@GO@SA nanocomposite.

[MB] ions	**(-) ΔH° (kJ/mol)**	**(-) ΔS° (J/mol.K)**	**(-) ΔG° (kJ/mol)**		
			298 K	**308 K**	**318 K**
33.5	37.8	105	7.00	5.24	4.53
50.0	39.5	147	5.70	4.02	3.00
100	27.7	80.0	4.00	3.03	2.32

ΔG° indicate the feasibility of MB removal onto Fe_3O_4@GO@SA at 25 °C. Furthermore, the rise in ΔG° with increasing temperature revealed that removal was more feasible at lower temperatures (25 °C) [66]. The negative values of ΔH° confirm that the adsorption process is exothermic and indicate the possibility of physical adsorption [67]. In addition, the values of ΔH° were in the range of −27.7 to −39.5 kJ/mol (ΔH°< 40 kJ/mol), indicating that the removal process was physisorption [68]. The negative ΔS° indicated that the disorder decreased at the solid/liquid interface during the removal process.

3.6. Reusability studies

To examine the durability of the Fe_3O_4@GO@SA nanocomposite, three reagents (0.01 M NaOH, 0.01 M HCl, and 0.01 M HNO_3) were utilized as the eluent as shown in Fig. 7**b**. Typically, each adsorption experiment consisted of 30 mg of Fe_3O_4@GO@SA adsorbent with 50 mL of 33.5 mg/L MB solution for 240 min. After the adsorption experiments, the MB-loaded Fe_3O_4@GO@SA adsorbent was magnetically separated, and the supernatant was used to determine the concentration of MB dye. The MB-loaded Fe_3O_4@GO@SA adsorbent was then treated with 50 mL of NaOH (0.01 M), HCl (0.01 M), and HNO_3 (0.01 M) and then shaken separately for 240 min. After that, the adsorbent was collected by a magnet. The % desorption of MB dye from Fe_3O_4@GO@SA was 88.6%, 31.5%, and 8. 00% using HCl (0.01 M), HNO_3 (0.01 M), and NaOH (0.01 M), respectively (Fig. 7**b**). This means that the strongest eluent for the regeneration of the adsorbent was HCl (0.01 M). In the four-cycle experiment (adsorption–desorption), the percentage of adsorption was 69%, which indicated that Fe_3O_4@GO@SA exhibited good reusability (Fig. 7**c**).

4. Conclusion

In this work, a novel magnetic nanocomposite (Fe3O4@GO@SA) was fruitfully fabricated through three steps: GO was first synthesized by a modified Hummers and Offeman approach, and then Fe_3O_4 graphene oxide (Fe_3O_4@GO) was synthesized through-loading magnetic nanoparticles on the GO surfaces by a chemical in situ coprecipitation method. After that, the carboxylic groups of Fe_3O_4@GO were reacted with the amino group of sulfanilic acid (SA) to produce a new magnetic nanocomposite (Fe_3O_4@GO@SA). The MB adsorption performance of the novel Fe_3O_4@GO@SA nanocomposite was evaluated. The optimization of all variables, such as the adsorbent mass, initial MB concentration, contact time, pH, and temperature, was investigated. The results revealed that the Fe_3O_4@GO@SA nanocomposite was successfully prepared. The Fe_3O_4@GO@SA nanocomposite showed a higher BET surface area (112 $m^2 \cdot g^{-1}$) than GO (3.30 $m^2 \cdot g^{-1}$) and MGO (95.2 $m^2 \cdot g^{-1}$). The adsorption of MB by Fe_3O_4@GO@SA displayed an adsorption capacity significantly higher than that by GO and MGO under optimum conditions (240 min; 0.0300 g (dose), pH 8, and 298 K). The monolayer removal capacity (qm) was reported to be 317 mg/g. The significant improvement is related to π-π interactions, Coulomb attraction, and H- bonding. Furthermore, the Langmuir and pseudo first-order models were reported to match the experimental findings for MB removal. Thermodynamic investigations confirmed that MB adsorption was spontaneous; in addition, MB adsorption displayed an exothermic characteristic. The regeneration and reusability studies demonstrated that the Fe_3O_4@GO@SA nanocomposite can be reused up to four runs successfully. Due to the high efficiency, the Fe_3O_4@GO@SA nanocomposite could be a promising adsorbent for eliminating MB dye from aquatic environments.

CRediT authorship contribution statement

Hassan M.A. Hassan: Conceptualization, Methodology, Investigation, Resources, Formal analysis, Supervision, Writing – review & editing. **M.R. El-Aassar:** Conceptualization, Methodology, Investigation, Formal analysis, Writing – original draft, Software, Validation, Writing – review & editing. **Mohammed A. El-Hashemy:** Methodology, Investigation, Formal analysis, Validation. **Mohamed A. Betiha:** Investigation, Formal analysis, Validation. **Alzaid:** Methodology, Investigation, Formal analysis, Validation. **Al Maha N. Al Qhobisi:** Investigation, Validation. **Linah A. Alzarea:** Investigation, Validation. **Ibrahim Hotan Alsohaimi:** Conceptualization, Methodology, Investigation, Resources, Formal analysis, Writing – original draft, Software, Validation.

Declaration of Competing Interest

The authors declare that they have no known competing financial interests or personal relationships that could have appeared to influence the work reported in this paper.

Acknowledgements

This work was funded by the Deanship of Scientific Research at Jouf University under grant No (DSR-2022-RG-0132).

References

[1] S.K. Sahoo, S. Padhiari, S.K. Biswal, B.B. Panda, G. Hota, Fe_3O_4 nanoparticles functionalized GO/g-C_3N_4 nanocomposite: an efficient magnetic nano-adsorbent for adsorptive removal of organic pollutants, Mater. Chem. Phys. 244 (2022), https://doi.org/10.1016/j.matchemphys.2020.122710 122710.
[2] Q. Li, Y. Li, X. Ma, Q. Du, K. Sui, D. Wang, C. Wang, H. Li, Y. Xia, Filtration and adsorption properties of porous calcium alginate membrane for methylene blue removal from water, Chem. Eng. J. 316 (2017) 623–630, https://doi.org/10.1016/j.cej.2017.01.098.
[3] NehalA. Salahuddin, HosnyA. EL-Daly, R.G. El Sharkawy, B.T. Nasr, Synthesis and efficacy of PPy/CS/GO nanocomposites for adsorption of ponceau 4R dye, Polymer (Guildf). 146 (2018) 291–303.
[4] X.-Y. Huang, H.-T. Bu, G.-B. Jiang, M.-H. Zeng, Cross-linked succinyl chitosan as an adsorbent for the removal of Methylene Blue from aqueous solution, Int. J. Biol. Macromol. 49 (2011) 643–651, https://doi.org/10.1016/j.ijbiomac.2011.06.023.
[5] Z.-W. Ma, K.-N. Zhang, Z.-J. Zou, Q.-F. Lü, High specific area activated carbon derived from chitosan hydrogel coated tea saponin: One-step preparation and efficient removal of methylene blue, J. Environ. Chem. Eng. 9 (2021), https://doi.org/10.1016/j.jece.2021.105251 105251.
[6] L.W. Jiang, F.T. Zeng, Y. Zhang, M.Y. Xu, Z.W. Xie, H.Y. Wang, H.L. Jiang, Preparation of a novel Fe_3O_4/graphite oxide nanosheet/citric acid-crosslinked β-cyclodextrin polymer composite to remove methylene blue from water, Adv. Powder Technol. 32 (2) (2021) 492–503. doi: 10.1016/j.apt.2020.12.026.
[7] D. Chen, H. Zhang, K. Yang, H. Wang, Functionalization of 4-aminothiophenol and 3-aminopropyltriethoxysilane with graphene oxide for potential dye and copper removal, J. Hazard. Mater. 310 (2016) 179–187, https://doi.org/10.1016/j.jhazmat.2016.02.040.
[8] R. Ahmad, K. Ansari, Comparative study for adsorption of congo red and methylene blue dye on chitosan modified hybrid nanocomposite, Process Biochem. 108 (2021) 90–102, https://doi.org/10.1016/j.procbio.2021.05.013.
[9] N. Nasuha, B.H. Hameed, P.U. Okoye, Dark-Fenton oxidative degradation of methylene blue and acid blue 29 dyes using sulfuric acid-activated slag of the steel-making process, J. Environ. Chem. Eng. 9 (2021) 104831.
[10] X. Li, Y. Liu, J. Wang, J. Gascon, J. Li, B. Van der Bruggen, Metal–organic frameworks based membranes for liquid separation, Chem. Soc. Rev. 46 (23) (2017) 7124–7144.
[11] G. Sun, C. Wang, W. Gu, Q. Song, A facile electroless preparation of Cu, Sn and Sb oxides coated Ti electrode for electrocatalytic degradation of organic pollutants, Sci. Total Environ. 772 (2021) 144908.
[12] Y. Fu, T. Viraraghavan, Fungal decolorization of dye wastewaters: a review, Bioresour. Technol. 79 (3) (2001) 251–262.
[13] S. Wang, H. Gao, L. Fang, Q. Hu, G. Sun, X. Chen, C. Yu, S. Tang, X. Yu, X. Zhao, Synthesis of novel CQDs/CeO2/SrFe12O19 magnetic separation photocatalysts and synergic adsorption-photocatalytic degradation effect for methylene blue dye removal, Chem. Eng. J. Adv. 6 (2021) 100089.
[14] M. Naushad, A.A. Alqadami, A.A. Al-Kahtani, T. Ahamad, M.R. Awual, T. Tatarchuk, Adsorption of textile dye using para-aminobenzoic acid modified activated carbon: Kinetic and equilibrium studies, J. Mol. Liq. (2019), https://doi.org/10.1016/j.molliq.2019.112075 112075.

[15] A.M. Aldawsari, I.H. Alsohaimi, A.A. Al-Kahtani, A.A. Alqadami, Z.E. Ali Abdalla, E.A.M. Saleh, Adsorptive performance of aminoterephthalic acid modified oxidized activated carbon for malachite green dye: mechanism, kinetic and thermodynamic studies, Sep. Sci. Technol. 56 (2021) 835–846, https://doi.org/10.1080/01496395.2020.1737121.
[16] A.A. Alqadami, M.A. Khan, M.R. Siddiqui, Z.A. Alothman, S. Sumbul, A facile approach to develop industrial waste encapsulated cryogenic alginate beads to sequester toxic bivalent heavy metals, J. King Saud Univ. - Sci. 32 (2020), https://doi.org/10.1016/j.jksus.2019.11.040.
[17] T. Maimaiti, R. Hu, H. Yuan, C. Liang, F. Liu, Q. Li, S.T. Yang, Magnetic Fe_3O_4/TiO_2/graphene sponge for the adsorption of methylene blue in aqueous solution, Diamond Related Mater. (2022). 108811, doi: 10.1016/j.diamond.2021.108811.
[18] F. Chen, W. Liang, X. Qin, L. Jiang, Y. Zhang, S. Fang, D. Luo, Preparation and recycled simultaneous adsorption of methylene blue and Cu^{2+} co-pollutants over carbon layer encapsulated Fe_3O_4/graphene oxide nanocomposites rich in amino and thiol groups, Colloids Surf., A 625 (2021), https://doi.org/10.1016/j.colsurfa.2021.126913 126913.
[19] M.Q. Seah, W.J. Lau, P.S. Goh, A.F. Ismail, Greener synthesis of functionalized-GO incorporated TFN NF membrane for potential recovery of saline water from salt/dye mixed solution, Desalination 523 (2022), https://doi.org/10.1016/j.desal.2021.115403 115403.
[20] F. Wang, L. Zhang, Y. Wang, X. Liu, S. Rohani, J. Lu, Fe_3O_4@ SiO_2@ CS-TETA functionalized graphene oxide for the adsorption of methylene blue (MB) and Cu (II), Appl. Surf. Sci. 420 (2017) 970–981, https://doi.org/10.1016/j.apsusc.2017.05.179.
[21] J.-L. Gong, Y.-L. Zhang, Y. Jiang, G.-M. Zeng, Z.-H. Cui, K. Liu, C.-H. Deng, Q.-Y. Niu, J.-H. Deng, S.-Y. Huan, Continuous adsorption of Pb(II) and methylene blue by engineered graphite oxide coated sand in fixed-bed column, Appl. Surf. Sci. 330 (2015) 148–157, https://doi.org/10.1016/j.apsusc.2014.11.068.
[22] Y. Li, Q. Du, T. Liu, J. Sun, Y. Wang, S. Wu, Z. Wang, Y. Xia, L. Xia, Methylene blue adsorption on graphene oxide/calcium alginate composites, Carbohydr. Polym. 95 (2013) 501–507, https://doi.org/10.1016/j.carbpol.2013.01.094.
[23] C. Qi, L. Zhao, Y. Lin, D. Wu, Graphene oxide/chitosan sponge as a novel filtering material for the removal of dye from water, J. Colloid Interface Sci. 517 (2018) 18–27, https://doi.org/10.1016/j.jcis.2018.01.089.
[24] L. Zhao, S.-T. Yang, S. Feng, Q. Ma, X. Peng, D. Wu, Preparation and application of carboxylated graphene oxide sponge in dye removal, Int. J. Environ. Res. Public Heal. 14 (2017), https://doi.org/10.3390/ijerph14111301.
[25] Z. Wu, H. Zhong, X. Yuan, H. Wang, L. Wang, X. Chen, G. Zeng, Y. Wu, Adsorptive removal of methylene blue by rhamnolipid-functionalized graphene oxide from wastewater, Water Res. 67 (2014) 330–344.
[26] J. He, G. Song, X. Wang, L. Zhou, J. Li, Multifunctional magnetic Fe3O4/GO/Ag composite microspheres for SERS detection and catalytic degradation of methylene blue and ciprofloxacin, J. Alloys Compd. 893 (2022), https://doi.org/10.1016/j.jallcom.2021.162226 162226.
[27] N. Tara, S.I. Siddiqui, R.K. Nirala, N.K. Abdulla, S.A. Chaudhry, Synthesis of antibacterial, antioxidant and magnetic Nigella sativa-graphene oxide based nanocomposite BC-GO@Fe3O4 for water treatment, Colloid Interface Sci. Commun. 37 (2020), https://doi.org/10.1016/j.colcom.2020.100281 100281.
[28] E. Yilmaz, H.İ. Ulusoy, Ö. Demir, M. Soylak, A new magnetic nanodiamond/graphene oxide hybrid (Fe_3O_4@ ND@ GO) material for pre-concentration and sensitive determination of sildenafil in alleged herbal aphrodisiacs by HPLC-DAD system, J. Chrom. B 1084 (2018) 113–121, https://doi.org/10.1016/j.jchromb.2018.03.030.
[29] D. Yuvali, I. Narin, M. Soylak, E. Yilmaz, Green synthesis of magnetic carbon nanodot/graphene oxide hybrid material (Fe_3O_4@ C-nanodot@ GO) for magnetic solid phase extraction of ibuprofen in human blood samples prior to HPLC-DAD determination, J. Pharm. Biomed. Anal. 179 (2020), https://doi.org/10.1016/j.jpba.2019.113001 113001.
[30] L. Fan, C. Luo, M. Sun, X. Li, F. Lu, H. Qiu, Preparation of novel magnetic chitosan/graphene oxide composite as effective adsorbents toward methylene blue, Bioresour. Technol. 114 (2012) 703–706, https://doi.org/10.1016/j.biortech.2012.02.067.
[31] H. Guo, K. Lin, Z. Zheng, F. Xiao, S. Li, Sulfanilic acid-modified P25 TiO2 nanoparticles with improved photocatalytic degradation on Congo red under visible light, Dye. Pigment. 92 (2012) 1278–1284, https://doi.org/10.1016/j.dyepig.2011.09.004.
[32] E.G. Söğüt, Y. Karataş, M. Gülcan, N.Ç. Kılıç, Enhancement of adsorption capacity of reduced graphene oxide by sulfonic acid functionalization: malachite green and Zn (II) uptake, Mater. Chem. Phys. 256 (2020), https://doi.org/10.1016/j.matchemphys.2020.123662 123662.
[33] S.I. El-Hout, S.M. El-Sheikh, H.M.A. Hassan, F.A. Harraz, I.A. Ibrahim, E.A. El-Sharkawy, A green chemical route for synthesis of graphene supported palladium nanoparticles: a highly active and recyclable catalyst for reduction of nitrobenzene, Appl. Catal. A Gen. 503 (2015) 176–185, https://doi.org/10.1016/j.apcata.2015.06.036.
[34] Y. Zhu, S. Murali, W. Cai, X. Li, J.W. Suk, J.R. Potts, R.S. Ruoff, Graphene and graphene oxide: synthesis, properties, and applications, Adv. Mater. 22 (2010) 3906–3924.
[35] A. Abu-Nada, A. Abdala, G. McKay, Isotherm and kinetic modeling of strontium adsorption on graphene oxide, Nanomater. 11 (2021), https://doi.org/10.3390/nano11112780.
[36] N.T. Vuong Hoan, N.T. Anh Thu, H.V. Duc, N.D. Cuong, D. Quang Khieu, V. Vo, Fe3O4/reduced graphene oxide nanocomposite: synthesis and its application for toxic metal ion removal, J. Chem. 2016 (2016) 1–10.
[37] Y. Gong, J. Su, M. Li, A. Zhu, G. Liu, P. Liu, Fabrication and adsorption optimization of novel magnetic core-shell chitosan/graphene oxide/β-cyclodextrin composite materials for bisphenols in aqueous solutions, Mater. 13 (2020), https://doi.org/10.3390/ma13235408.
[38] H. Bhandari, R. Srivastav, V. Choudhary, S.K. Dhawan, Enhancement of corrosion protection efficiency of iron by poly(aniline-co-amino-naphthol-sulphonic acid) nanowires coating in highly acidic medium, Thin Solid Films 519 (2010) 1031–1039, https://doi.org/10.1016/j.tsf.2010.08.038.
[39] M. Srimathi, R. Rajalakshmi, S. Subhashini, Polyvinyl alcohol–sulphanilic acid water soluble composite as corrosion inhibitor for mild steel in hydrochloric acid medium, Arab. J. Chem. 7 (2014) 647–656, https://doi.org/10.1016/j.arabjc.2010.11.013.
[40] A.A. Alqadami, M.A. Khan, M. Otero, M.R. Siddiqui, B.-H. Jeon, K.M. Batoo, A magnetic nanocomposite produced from camel bones for an efficient adsorption of toxic metals from water, J. Clean. Prod. 178 (2018), https://doi.org/10.1016/j.jclepro.2018.01.023.
[41] M.A. Khan, A.A. Alqadami, M. Otero, M.R. Siddiqui, Z.A. Alothman, I. Alsohaimi, M. Rafatullah, A.E. Hamedelniel, Heteroatom-doped magnetic hydrochar to remove post-transition and transition metals from water: synthesis, characterization, and adsorption studies, Chemosphere 218 (2019) 1089–1099, https://doi.org/10.1016/j.chemosphere.2018.11.210.
[42] M. Khaleghi-Abbasabadi, D. Azarifar, Magnetic Fe3O4-supported sulfonic acid-functionalized graphene oxide (Fe3O4@GO-naphthalene-SO3H): a novel and recyclable nanocatalyst for green one-pot synthesis of 5-oxo-dihydropyrano[3,2-c]chromenes and 2-amino-3-cyano-1,4,5,6-tetrahydropyrano[3,2-c]qui, Res. Chem. Intermed. 45 (2019) 2095–2118, https://doi.org/10.1007/s11164-018-03722-y.
[43] Y.-X. Ma, W.-J. Shao, W. Sun, Y.-L. Kou, X. Li, H.-P. Yang, One-step fabrication of β-cyclodextrin modified magnetic graphene oxide nanohybrids for adsorption of Pb(II), Cu(II) and methylene blue in aqueous solutions, Appl. Surf. Sci. 459 (2018) 544–553, https://doi.org/10.1016/j.apsusc.2018.08.025.
[44] R. Sedghi, B. Heidari, M. Yassari, Novel molecularly imprinted polymer based on β-cyclodextrin@graphene oxide: Synthesis and application for selective diphenylamine determination, J. Colloid Interface Sci. 503 (2017) 47–56, https://doi.org/10.1016/j.jcis.2017.05.013.
[45] R. Siburian, H. Sihotang, S. Lumban Raja, M. Supeno, C. Simanjuntak, New route to synthesize of graphene nano sheets, Orient. J. Chem 34 (1) (2018) 182–187.
[46] H.O. Onset, J. Sui, The effects of KCl, NaCl and K 2 CO 3 on the, Oxid. Met. 85 (2016) 565–598.
[47] A.A. Alqadami, M. Naushad, Z.A. ALOthman, M. Alsuhybani, M. Algamdi, Excellent adsorptive performance of a new nanocomposite for removal of toxic Pb(II) from aqueous environment: Adsorption mechanism and modeling analysis, J. Hazard. Mater. 389 (2020) 121896, 10.1016/j.jhazmat.2019.121896.
[48] D. Li, T. Hua, J. Yuan, F. Xu, Methylene blue adsorption from an aqueous solution by a magnetic graphene oxide/humic acid composite, Colloids Surfaces A Physicochem. Eng. Asp. 627 (2021), https://doi.org/10.1016/j.colsurfa.2021.127171 127171.
[49] V. Georgakilas, J.N. Tiwari, K.C. Kemp, J.A. Perman, A.B. Bourlinos, K.S. Kim, R. Zboril, Noncovalent functionalization of graphene and graphene oxide for energy materials, biosensing, catalytic, and biomedical applications, Chem. Rev. 116 (2016) 5464–5519, doi: 10.1021/acs.chemrev.5b006 20.
[50] T. Ma, Y. Wu, N. Liu, Y. Wu, Hydrolyzed polyacrylamide modified diatomite waste as a novel adsorbent for organic dye removal: adsorption performance and mechanism studies, Polyhedron 175 (2020), https://doi.org/10.1016/j.poly.2019.114227 114227.
[51] Munasir, R.P. Kusumawati, D.H. Kusumawati, Kusumawati, Magnetic Properties of Fe3O4@Graphene: preparation from Natural Material, J. Phys. Conf. Ser. 1569 (4) (2020) 042087.
[52] T.H. Do, V.T. Nguyen, N.Q. Dung, M.N. Chu, D. Van Kiet, T.T.K. Ngan, L. Van Tan, Study on methylene blue adsorption of activated carbon made from Moringa oleifera leaf, Mater. Today Proc. 38 (2021) 3405–3413, https://doi.org/10.1016/j.matpr.2020.10.834.
[53] A. Maleki, M. Mohammad, Z. Emdadi, N. Asim, M. Azizi, J. Safaei, Adsorbent materials based on a geopolymer paste for dye removal from aqueous solutions, Arab. J. Chem. 13 (2020) 3017–3025, https://doi.org/10.1016/j.arabjc.2018.08.011.
[54] M. Naushad, A.A. Alqadami, Z.A. AlOthman, I.H. Alsohaimi, M.S. Algamdi, A.M. Aldawsari, Adsorption kinetics, isotherm and reusability studies for the removal of cationic dye from aqueous medium using arginine modified activated carbon, J. Mol. Liq. 293 (2019), https://doi.org/10.1016/j.molliq.2019.111442 111442.
[55] Über die Adsorption in Lösungen, Zeitschrift Für Phys, Chemie. 57U (1907) 385, https://doi.org/10.1515/zpch-1907-5723.
[56] A. Wallis, M.F. Dollard, Local and global factors in work stress - The Australian dairy farming examplar, Scand. J. Work. Environ. Heal. Suppl. (2008) 66–74.
[57] D.-W. Cho, B.-H. Jeon, C.-M. Chon, F.W. Schwartz, Y. Jeong, H. Song, Magnetic chitosan composite for adsorption of cationic and anionic dyes in aqueous solution, J. Ind. Eng. Chem. 28 (2015) 60–66.
[58] C. Păcurariu, O. Paşka, R. Ianoş, S.G. Muntean, Effective removal of methylene blue from aqueous solution using a new magnetic iron oxide nanosorbent prepared by combustion synthesis, Clean Technol. Environ Policy 18 (2016) 705–715, https://doi.org/10.1007/s10098-015-1041-7.
[59] E.A. El-Sharkaway, R.M. Kamel, I.M. El-Sherbiny, S.S. Gharib, Removal of methylene blue from aqueous solutions using polyaniline/graphene oxide or

polyaniline/reduced graphene oxide composites, Environ. Technol. 41 (2020) 2854–2862, https://doi.org/10.1080/09593330.2019.1585481.
[60] T. Huang, M. Yan, K. He, Z. Huang, G. Zeng, A. Chen, M. Peng, H. Li, L. Yuan, G. Chen, Efficient removal of methylene blue from aqueous solutions using magnetic graphene oxide modified zeolite, J. Colloid Interface Sci. 543 (2019) 43–51, https://doi.org/10.1016/j.jcis.2019.02.030.
[61] G. Liu, N. Wang, J. Zhou, A. Wang, J. Wang, R. Jin, H. Lv, Microbial preparation of magnetite/reduced graphene oxide nanocomposites for the removal of organic dyes from aqueous solutions, RSC Adv. 5 (2015) 95857–95865, https://doi.org/10.1039/C5RA18136D.
[62] A.S. Dehghan, K. Mehdi, T. Roghayeh, H. Morteza, S. Abbas, G.M.R., Fast removal of methylene blue from aqueous solution using magnetic-modified Fe3O4 nanoparticles, J. Environ. Eng. 141 (2015) 4014049, https://doi.org/10.1061/(ASCE)EE.1943-7870.0000878.
[63] L. Thi Mong Thy, N. Hoan Kiem, T. Hoang Tu, L. Minh Phu, D. Thi Yen Oanh, H. Minh Nam, M. Thanh Phong, N.H. Hieu, Fabrication of manganese ferrite/graphene oxide nanocomposites for removal of nickel ions, methylene blue from water, Chem. Phys. 533 (2020) 110700, doi: 10.1016/j.chemphys.2020.110700.
[64] H.V. Tran, L.T. Hoang, C.D. Huynh, An investigation on kinetic and thermodynamic parameters of methylene blue adsorption onto graphene-based nanocomposite, Chem. Phys. 535 (2020), https://doi.org/10.1016/j.chemphys.2020.110793 110793.
[65] S. Lagergren, About the theory of so-called adsorption of soluble substances, Handlingar. 24 (1898) 1–39.
[66] A. Ashrafi, A. Rahbar-Kelishami, H. Shayesteh, Highly efficient simultaneous ultrasonic assisted adsorption of Pb (II) by Fe3O4@MnO2 core-shell magnetic nanoparticles: synthesis and characterization, kinetic, equilibrium, and thermodynamic studies, J. Mol. Struct. 1147 (2017) 40–47, https://doi.org/10.1016/j.molstruc.2017.06.083.
[67] S. Melhi, M. Algamdi, A.A. Alqadami, M.A. Khan, E.H. Alosaimi, Fabrication of magnetically recyclable nanocomposite as an effective adsorbent for the removal of malachite green from water, Chem. Eng. Res. Des. 177 (2022) 843–854, https://doi.org/10.1016/j.cherd.2021.11.028.
[68] M.A. Khan, S.M. Wabaidur, M.R. Siddiqui, A.A. Alqadami, A.H. Khan, Silico-manganese fumes waste encapsulated cryogenic alginate beads for aqueous environment de-colorization, J. Clean. Prod. 244 (2020), https://doi.org/10.1016/j.jclepro.2019.118867.